# The thermal history effect on shear band initiation in metallic glass

Cite as: J. Appl. Phys. **119**, 245113 (2016); https://doi.org/10.1063/1.4954873
Submitted: 11 April 2016 . Accepted: 14 June 2016 . Published Online: 30 June 2016

S. Wang, Y. F. Ye, S. Q. Shi, and Y. Yang

JOURNAL OF APPLIED PHYSICS **119**, 245113 (2016)

# The thermal history effect on shear band initiation in metallic glass

S. Wang,[1,2,a)] Y. F. Ye,[1] S. Q. Shi,[2,a)] and Y. Yang[1,a)]
[1]*Department of Mechanical and Biomedical Engineering, Centre for Advanced Structural Materials, City University of Hong Kong, Kowloon Tong, Kowloon, Hong Kong*
[2]*Department of Mechanical Engineering, The Hong Kong Polytechnic University, Hung Hom, Kowloon, Hong Kong*

(Received 11 April 2016; accepted 14 June 2016; published online 30 June 2016)

The effect of thermal history on shear band initiation in metallic glass is investigated with spherical nanoindentation. Our results clearly show that the indentation size effect on the metallic-glass hardness varies systematically with the thermal history, which is in excellent agreement with the softening-induced shear-band initiation model we recently developed. On a fundamental level, the outcome of our research establishes a correlation between the shear modulus and the critical length scale for initiating an autocatalytic shear-band growth in metallic glasses. *Published by AIP Publishing.*
[http://dx.doi.org/10.1063/1.4954873]

## I. INTRODUCTION

Yielding in metallic glasses (MGs) at low temperatures is caused mainly by shear banding, which is essentially a process of thermo-mechanical or mechanical instability that entails initiation and propagation of bona fide shear bands within an amorphous structure.[1–16] In principle, shear band initiation is triggered by shear softening, a physical process often being attributed to the production of excess free volumes,[2] shear transformation zones,[1] or other "defect-like" regions[17–26] under stress that cause local dilation. From a thermodynamic viewpoint, this softening process is equivalent to stress-induced glass transition,[7,27] which leads to the reduction of local viscosity.[8,27–29] Consequently, shear banding occurs because of shear thinning.[27] From a mechanistic stand point of view, shear-band initiation entails subcritical growth of shear-band "embryos," which are essentially nano-sized shear bands initially growing in a stable manner until reaching a critical size that triggers the autocatalytic growth.[4] In the MG literature,[9–12] different models were employed or developed to predict the criticality of shear-band initiation. For example, shear-band initiation was previously modeled as a result of local temperature surge by Shimizu *et al.*[9] or as a process of local fracture by Volkert *et al.*,[10] Jang and Greer,[11] and Cheng *et al.*[12,16]

Recently, based on the nonlinear earthquake mechanics,[30] we also developed a softening model for shear-band initiation in MGs. Unlike the previous modeling, an embryonic shear band in our model was taken to be a nano-sized shear crack with a frictional wake. In other words, we take into account a remnant strength left in the shear-banding region after shear softening, which contrasts an ordinary shear crack with only stress-free surfaces. Based on our model, a spherical indentation approach was devised to probe shear-band initiation in MGs. According to our previous results, shear-band initiation is strain rate dependent, which is consistent with the later finding by Tonnies *et al.*,[13] and the critical length scale for shear-band initiation can be related to the indentation size effect in MGs.[14] On the other hand, according to the prior results,[31] it was known that thermal annealing can lead to the embrittlement of MGs.[32] Since thermal annealing causes structural relaxation, it can be envisioned that a relaxed glassy state might make shear-band initiation difficult, therefore in favor of brittle fracture. In the current study, our interest is to extend our previous work to investigate how shear-band initiation can be possibly affected by the thermal history of a MG.

## II. EXPERIMENT

For a systematic study of the thermal history effect, a Zr-based MG with the nominal composition of $Zr_{52.5}Ti_5Cu_{17.9}Ni_{14.6}Al_{10}$ (in atomic percentage) was selected as the model material. Ribbon samples were prepared via melt-spinning at an estimated cooling rate of $\sim 10^5$ K/s (Ref. 33), and bulk samples were prepared via the conventional copper-mold casting method with the estimated cooling rate of $\sim 10^2$–$10^3$ K/s.[33] According to the previous study,[34] the glass transition temperature $T_g$ of the as-cast bulk samples is around 693 K. Subsequently, some of the as-cast samples were annealed at ~653 K for 61 h and 256 h, respectively. To ensure the structural amorphousness of all MG samples, X-Ray Diffractometry (XRD, Cu radiation) analyses were carried out. As shown in Fig. 1(a), the XRD patterns only display a broad diffraction maximum without any detectable sharp Bragg peaks, indicative of an overall amorphous structure for the samples investigated.

Afterwards, a series of spherical indentation experiments were carried out on the Hysitron™ Nanoindentation System. For a systematic investigation of the indentation size effect, the following tip radii were used: 2 $\mu$m, 5 $\mu$m, 10 $\mu$m, and 20 $\mu$m. Note that the tip radii of the spherical indenters were calibrated before the tests, details of which have been described in Ref. 14 but omitted here for brevity. To avoid the possible strain rate effect,[13,14] the indentation strain rate $\dot{\varepsilon}_h = \dot{P}/(2P)$ was set at the constant of $0.5\,s^{-1}$,

a)Authors to whom correspondence should be addressed. Electronic addresses: songwang4@cityu.edu.hk; mmsqshi@polyu.edu.hk; and yonyang@cityu.edu.hk.

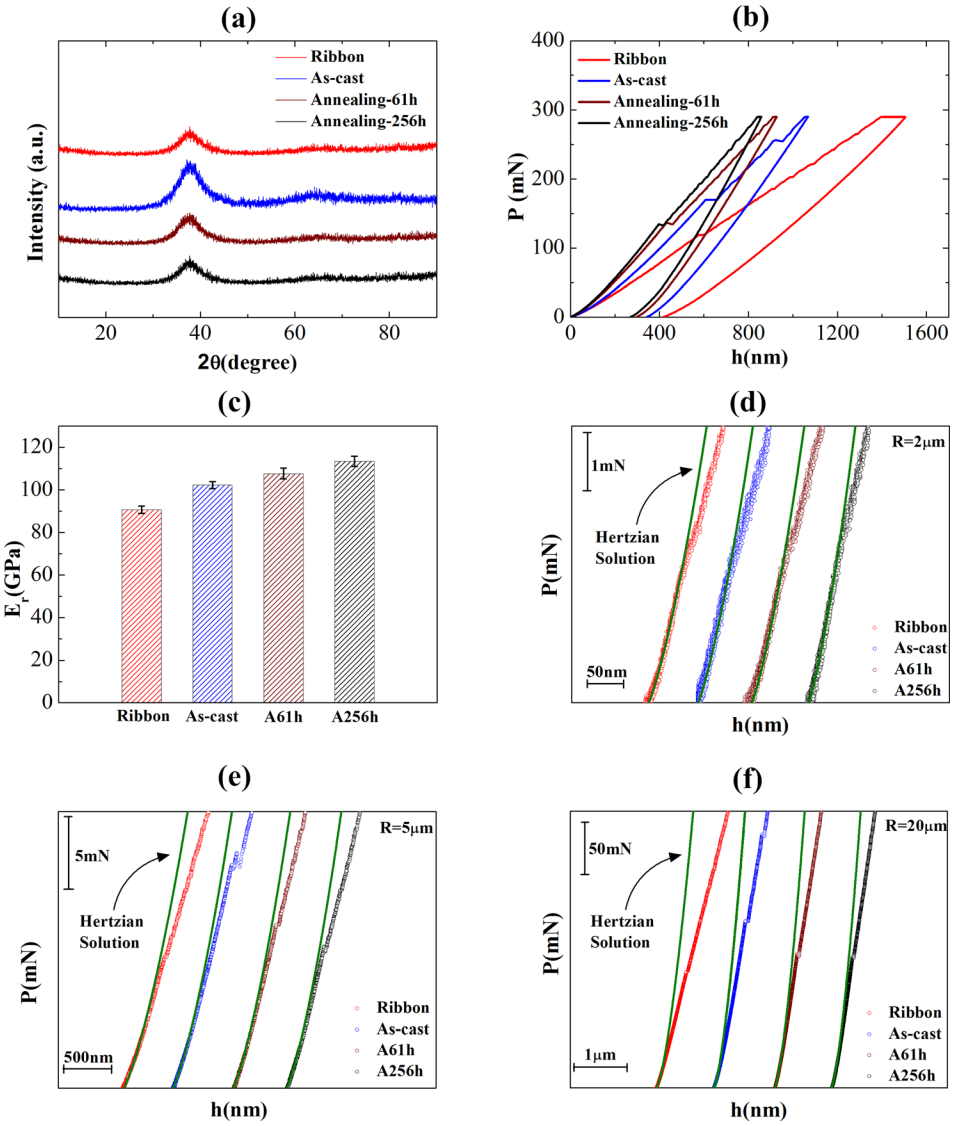


FIG. 1. (a) The XRD patterns of the MGs with various thermal histories, (b) the typical indentation load ($P$)-displacement ($h$) curves of the MGs, (c) the comparison of the reduced modulus ($E_r$) extracted from the spherical P-h curves, and the indentation loading curves obtained at the indenter radius of (d) 2 $\mu$m, (e) 5 $\mu$m, and (f) 20 $\mu$m for $\dot{\varepsilon}_h = 0.5\,s^{-1}$ in comparison with the Hertzian theory (the green solid curve). Note that A61h and A256h stand for the samples annealed for 61 h and 256 h, respectively.

where $\dot{P}$ is the indentation loading rate and $P$ is the indentation load. For simplicity, unloading was programmed to follow a constant unloading rate. Fig. 1(b) displays the typical load-displacement *(P-h)* curves obtained from indenting the four types of MG samples to the same peak load of 300 mN with the indenter of the radius $R = 20$ $\mu$m. Evidently, it can be inferred from the shape of the loading curves that the elastic modulus of the samples varies with the thermal history with the ribbon sample being the softest and the bulk sample annealed for 256 h the stiffest. Following the method detailed in Ref. 14, we can fit the initial elastic portion of the indentation loading curve to the Hertzian solution to extract the reduced modulus $E_r$. As shown in Fig. 1(c), $E_r = 91 \pm 2$ GPa for the ribbon sample, $102 \pm 2$ GPa for the as-cast sample, $108 \pm 2$ GPa for the sample annealed for 61 h, and $113 \pm 2$ GPa for the sample annealed for 256 h, which is consistent with our observations [Fig. 1(b)].

## III. RESULTS AND DISCUSSION

### A. Indentation size effect

Figures 1(d)–1(f) show the indentation loading curves obtained from different tip radii in comparison with the Hertzian solutions. It is worth noting that, at the small tip radius (such as $R = 2$ $\mu$m), the departure of the loading curve from the Hertzian solution coincides with the first pronounced "pop-in" event as shown in Fig. 1(d), which is consistent with the previous studies;[15,35] however, as the tip radius increases, the departure point seemingly precedes the first pronounced "pop-in" point on the loading curve [Figs. 1(e) and 1(f)]. Similar behaviors were also observed in the prior work.[14,36] For consistency, the yielding load $P_y$ is herein taken to be the departure point. As a result, the yielding pressure or hardness $p_c$ of the MG sample can be derived as $p_c = \left(\frac{6P_yE_r^2}{\pi^3R^2}\right)^{\frac{1}{3}}$ according to the Hertzian theory.

Figs. 2(a)–2(d) show the plot of $p_c$ versus $R$ for the four types of MG samples. Note that at least 10 indentation tests were conducted for each data point shown in Figs. 2(a)–2(d). As shown in these figures, an indentation size effect is evident for all the MG samples and the yielding pressure $p_c$ obtained from the same tip radius ranks across different MG samples in the same order as their elastic moduli [Fig. 1(c)]. On the basis of the prior works,[5,14–16,35,36] yielding under a spherical indenter can be rationalized as a result of the autocatalytic growth of an embryonic shear-band. As a result, the

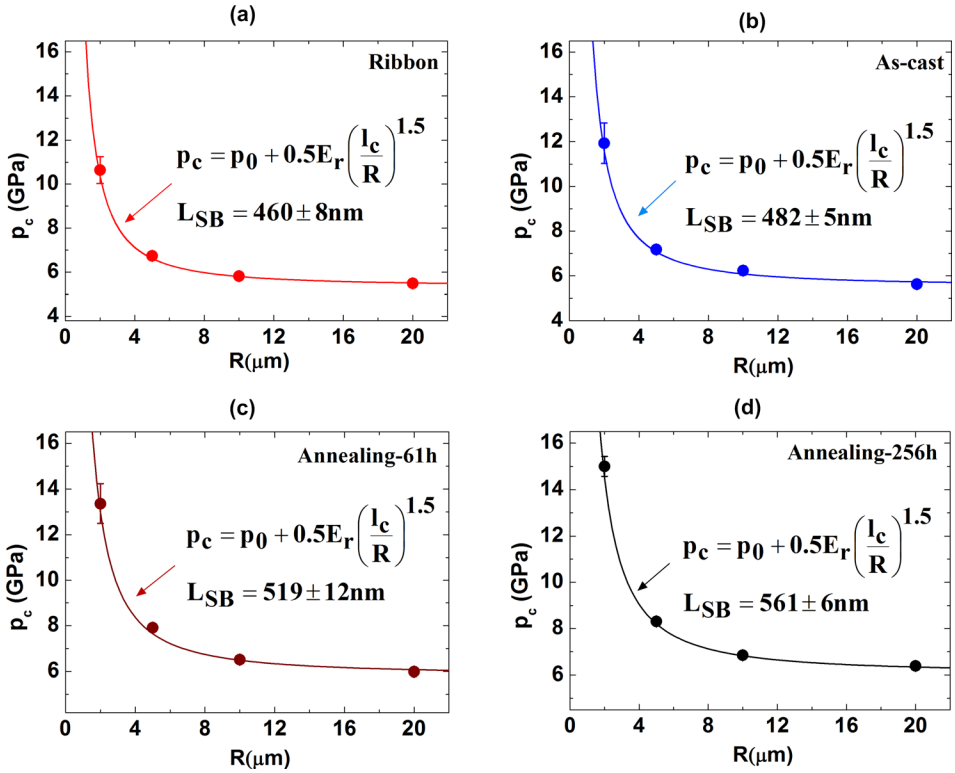


FIG. 2. The indentation size effect for (a) the ribbon sample, (b) the as-cast bulk sample, (c) the bulk sample annealed for 61 h, and (d) the bulk sample annealed for 256 h. Note that all experimental data can be fitted very well with the theoretical model we developed.[14]

following scaling relation can be derived based on the nonlinear fracture mechanics:[14,30] $p_c = p_0 + C_0 E_r \left(\frac{L_{SB}}{R}\right)^{C_1}$, in which $L_{SB}$ is the critical length scale that triggers the autocatalytic shear-band growth; $p_0$ is the size-insensitive yielding pressure that depends on the chemical composition of the material while $C_0$ and $C_1$ are the chemistry-insensitive parameters that may be viewed as two constants ($C_0 \sim 0.5$ and $C_1 \sim 1.5$). For brevity, the derivation of the scaling relation is omitted here, and interested readers are referred to Ref. 14 for details. Here, it should be emphasized that, as stated in our previous work,[14] homogeneous initiation of shear instability becomes unlikely with the decreasing tip radius. Once the local plastic zone grows to a sample surface before instability occurs, heterogeneous initiation of shear instability would take place. Consequently, the above scaling relation becomes invalid for a very small tip radius. According to our previous measurements, this critical tip radius is around 1 $\mu$m for the Zr-based MG. To understand this phenomenon across different MGs, further extensive experiments are needed which will be discussed in our future work. By taking $p_0$ and $L_{SB}$ as the fitting parameters, we can fit the experimental data to the above scaling relation. As shown in Figs. 2(a)–2(d), it can be seen that the trend of the experimental data can be captured very well by our model. As a result, we can obtain $p_0$ and $L_{SB}$ for the different MG samples, as tabulated in Table I.

From Table I, we can see that the extracted size-independent hardness $p_0$ of the MG samples varies systematically with their thermal history, increasing from ~5.35 GPa for the ribbon sample to ~6.06 GPa for the bulk sample annealed for 256 h. However, regardless of the thermal history, the ratio of $p_0/3E$ remains to be almost a constant ~0.018 for all the MG samples tested. Since the yielding strength $\sigma_y$ of a MG is usually approximated as one third of the corresponding hardness $p_0/3$, the constancy of $p_0/3E$ indicates that, in the absence of the indentation size effect, yielding in the MG is controlled by a constant strain of ~0.018. This finding is consistent very well with the previous experimental results.[3,37–39] Now, let us discuss the critical length $L_{SB}$ obtained by data fitting for the shear-band initiation in the Zr-based MG. According to the previous data obtained from micro-/nano-compression[10,37,40–43] and nano-tension,[11,38,44] it was estimated that, once the sample dimension is within the range from ~100 to ~400 nm, homogeneous-like or distributed plasticity can be observed without pronounced shear localization in MGs. These length scales were commonly interpreted as a critical size for nucleating a shear band. By comparison, the length scales $L_{SB}$ extracted from the current study are about 25%–400% higher. This discrepancy indicates that, unlike uniaxial loading, yielding in the MGs under spherical indentation is not controlled by the immediate presence of an embryonic shear band. This is plausible since indentation-induced hydrostatic pressure can stabilize the growth of any crack-like defects, thereby prolonging the stage of its subcritical growth.[45] As a result, the critical length scale for shear-band initiation becomes lengthened. Here, it is worth noting that distributed plasticity was also observed in the Zr-based MG thin films with a thickness ranging from 600 nm to 1 $\mu$m.[37,39,42] Given the report of large compressive residual stresses (1–2 GPa) in the MG thin films,[37] we consider that the observation of the distributed plasticity in the MG thin films supports the $L_{SB}$ values we obtained from the spherical indentation. Furthermore, according to the recent work of Perepezko *et al.*,[46] yielding in MGs under spherical indentation may entail the initiation of multiple shear bands; if that was the case, one could envision that

TABLE I. The reduced modulus ($E_r$), Young's modulus ($E$), size-insensitive yielding pressure ($p_o$), and the critical length scale ($L_{SB}$) extracted from our spherical indentation tests for the different MG samples. Note that the Poisson's ratio $\nu = 0.37$ is used to convert $E_r$ to $E$.

| Sample | $E_r$ (GPa) | $E$ (GPa) | $p_0$ (GPa) | $p_0/3E$ | $L_{SB}$ (nm) |
|---|---|---|---|---|---|
| Ribbon | 91 ± 2 | 85 ± 2 | 5.35 ± 0.02 | 0.021 ± 0.003 | 460 ± 8 |
| As-cast bulk | 102 ± 2 | 97 ± 2 | 5.54 ± 0.01 | 0.019 ± 0.002 | 482 ± 5 |
| Annealed bulk for 61 h | 108 ± 2 | 103 ± 3 | 5.85 ± 0.02 | 0.019 ± 0.002 | 519 ± 12 |
| Annealed bulk for 256 h | 113 ± 2 | 109 ± 2 | 6.06 ± 0.01 | 0.018 ± 0.002 | 561 ± 6 |

the critical length scale for shear band initiation under spherical indentation should be longer than that under uniaxial loadings, the latter of which usually involves only the initiation of one shear band. Therefore, the discrepancy between the critical length scales extracted from different experiments may be also attributed to the possible stress state effect.

Before proceeding, we would like to further discuss the physical meaning of shear band initiation and the length scale we extracted. According to the prior experimental[10,11,40,42–44] and computational[9,47] results, shear band initiation was usually associated with the transition from a homogeneous deformation to inhomogeneous (shear-banding) deformation in a uniaxial test, either tension or compression, with the transition size ranging from ~100 nm to ~400 nm. However, there were also experimental reports that shear banding still prevailed at the length scale of ~100 nm;[41,48–51] the recent computational simulation[9,47] even showed that shear banding can be observed down to the length scale of 10 nm. These theoretical/computational findings seem contradictory to each other, suggesting that the issue of shear band initiation is controversial and has not been fully settled yet. To reconcile this controversy, one plausible explanation is that the homogeneous deformation observed at the small size scale be indeed caused by distributed shear banding. However, unlike the macroscopic shear band growing at a speed close to the sound speed,[52–54] the individual small-sized shear band must propagate much more slowly, or undergo a subcritical growth stage, in order to make this mechanism of distributed shear banding effective. In other words, the so-called shear band initiation could be a transition from a slowly growing to a fast growing shear band. Because of the low growing speed of the small shear band, it is possible that homogeneous-like deformation (or multiple shear banding) can be observed if the applied strain rate exceeds the strain-carrying capacity of a single small shear band or inhomogeneous shear banding be observed if the applied strain rate is within the strain-carrying capacity of the single small shear band. This rate dependent scenario of "shear band initiation" was early proposed by Schuh *et al.*[55] to explain the disappearance of pop-ins in the indentation tests and was indeed observed recently by Tonnies *et al.*[56] in nano- and micro-compression tests. Our recent work also showed that shear band initiation,[14] i.e., the transition from multiple stably growing shear bands to a single runaway shear band, is rate dependent also in spherical indentation. Back to our current work, we define an embryonic shear band as a shear band constrained underneath the indenter, which is yet to reach the runaway speed.

### B. The theory

By treating the embryonic shear band as a constrained shear band, here we provide a theoretical estimate of the critical length scale $L_{SB}$ following the model developed by Uenishi and Rice[30] for the initiation of an earthquake, which is essentially a fault with shear softening analogous to a shear band. For the simple case of linear softening,[30] mechanical instability is triggered once the fault size reaches $\alpha G/\Theta$, where $\alpha \sim 1.16$ is a dimensionless factor, $G$ is the shear modulus of the elastic surrounding of the fault; $\Theta$ is the linear softening rate within the fault, which is defined as $\Theta = \Delta\sigma_c/\delta$. Here, $\Delta\sigma_c$ denotes the total strength drop due to shear softening and $\delta$ is the critical shear displacement over which shear softening is completed. For a shear band with a thickness $t_{SB}$, we can define a shear softening rate $W = \Delta\sigma_c/\Delta\gamma$ (see the inset of Fig. 3), $\Delta\gamma = \delta/t_{SB}$ is the range of the shear strain that can be keyed to shear softening. Equating $L_{SB}$ to the above theoretical estimates gives a simple dimensionless relation

$$\frac{L_{SB}}{t_{SB}} = \alpha\left(\frac{G}{W}\right). \tag{1}$$

According to the above equation, the ratio of $L_{SB}/t_{SB}$ scales with $G/W$. Here, $t_{SB}$ can be regarded as a constant for real MGs (10–20 nm) according to Refs. 57 and 58, and the softening rate $W$ is strain rate dependent according to Ref. 14. In principle, $t_{SB}$ and $W$ may also be affected by thermal annealing. However, for simplicity, we consider that the annealing effect on $t_{SB}$ is secondary and negligible compared to that on $G$.

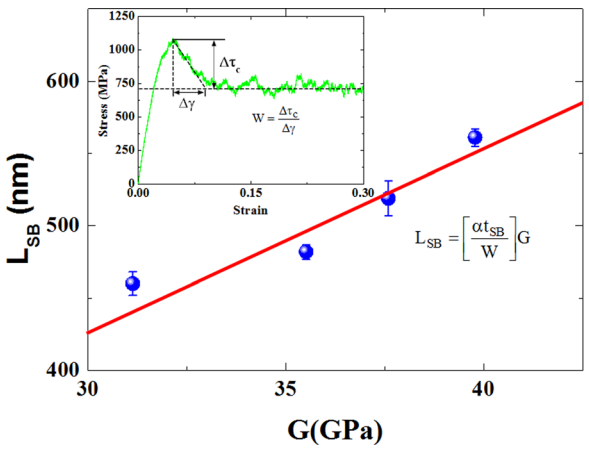


FIG. 3. The plot of $L_{SB}$ versus $G$ that can be fitted very well to a linear correlation. (inset: the shear stress–strain curve obtained from the recent MD simulation[14] showing the shear softening in the $Zr_{50}Cu_{50}$ MG after yielding).

To verify Eq. (1), $L_{SB}$ is plotted against $G$ in Fig. 3. Evidently, the data of $L_{SB}$ versus $G$ can be well fitted to a linear correlation, therefore corroborating our hypothesis. From the slope of this trend line (Fig. 3), we obtain $\alpha t_{SB}/W \sim 14$. Thus, the linear softening rate $W$ is extracted to be $\sim$1.4 GPa for $t_{SB} = 20$ nm or $\sim$0.7 GPa for $t_{SB} = 10$ nm. The dependence of $L_{SB}$ on $G$ implies that it becomes difficult for a shear-band embryo to develop into a bona fide shear band should the former be surrounded by a stiffer elastic medium. In other words, shear banding becomes more difficult in an annealed MG since thermal annealing generally elevates its elastic modulus, thus in favor of brittle fracture as revealed by the previous experiments.[5,31,32,59] Now we would like to have a further discussion on the thermal effect on $W$. According to the prior work,[60,61] the stress overshoot can be suppressed once the quenching rate is fast enough. In such a case, there is limited or even no shear softening. Since shear banding stems from shear softening, shear banding is therefore effectively suppressed by the fast quenching rate. Back to our model, if the softening rate $W$ approaches zero, the critical length scale for shear band instability will go to infinity. Theoretically, this signals the case of "no shear banding" or homogeneous deformation. In general, one can expect a reduction in $W$ in a ribbon sample. To check this, we carefully examined the shear softening rate $W$ for the samples with different thermal histories. According to Equation (1), the softening rate $W$ for the ribbon sample is estimated to be $\sim$1.35 GPa if we take $t_{SB} = 20$ nm, while $W \sim 1.45$ GPa for the other bulk samples. This is consistent with the general expectation.

Next, we compare the extracted $W$ with the reported data from either atomistic simulations or experiments. As listed in Table II, it can be seen that the softening rate $W$ is material dependent and generally varies with temperature and strain rate. Despite these variations, it is evident that the softening rate $W$ increases with the decreasing strain rate, which agrees with the previous findings.[14] Compared to the data obtained experimentally by Nieh *et al.*[62] and Lu *et al.*,[63] which range from $\sim$1 GPa to $\sim$2 GPa at the shear strain rate of 0.75 $s^{-1}$ or 0.0075 $s^{-1}$, it can be seen that our extracted $W$ agrees very well with these data obtained at the temperatures close to the glass transition point. Again, this is reasonable and further corroborates the idea that yielding or shear-banding in MGs is thermodynamically equivalent to a local stress-induced glass transition process.[64,65]

In the previous study,[66] it was shown that a rejuvenated glass tends to exhibit the trend of homogeneous deformation more than a relaxed glass, which seemingly suggests that, if the homogeneous deformation was controlled by shear band initiation, rejuvenated MGs or MGs with a faster quenching rate should possess a larger critical length for shear band initiation. However, according to the literature,[5,11,12,56,67,68] there could be two types of homogeneous deformations. One is a genuine homogenous flow without shear banding and the other, also termed as distributed plasticity,[5,68] involves multiple finely spaced shear banding. In theory, one can envision that a larger critical length is more beneficial to the first type of homogenous deformation while a smaller critical length is more beneficial to the second type. However, we have not done any size effect study yet at the current time which could provide us the clue for which mechanism is responsible for homogenous-like deformation in our metallic glasses. Furthermore, we should also stress that the critical length scales with the ratio of $G/W$. For our ribbon sample, we found that $G$ reduces more significantly than $W$ with the cooling rate, which leads to a smaller critical length in the ribbon samples. However, in other type of ribbon samples, one may observe a reverse trend if $W$ is affected by the cooling rate more than $G$. At the present time, we are inclined to view this as an open problem, which will be addressed in our future work.

Before proceeding to summary, it is worth mentioning a recent work of Wang *et al.*,[67] in which shear band initiation was modeled from an energy balance perspective. While our model was developed from the perspective of mechanical equilibrium, both studies indeed share similar results. In Wang's work, they assumed that the energy needed to create a shear band is provided by the release of elastic energy when yielding occurs, and that the onset of yielding is associated with a stress drop from the stress needed to initiate a shear band to the flow stress retained during shear-band sliding. In our model, the growing front of the shear fault or shear-band embryo comes about with shear softening, which causes the local stress drop and thus elastic energy release from the local surrounding materials. From a dimensional analysis, the elastic energy released must be scaled with the

TABLE II. Comparison of the shear softening rate $W$ obtained from the previous experiments and simulations. Note that the unit of $W$ is GPa and the abbreviations "Sim." and "Exp." stand for simulation and experiment, respectively. Note that the strain rate herein refers to the shear component.

| | | $T$ (K) | | | |
|---|---|---|---|---|---|
| | $\dot{\varepsilon}(s^{-1})$ | 50 | 100 | 663 | 683 |
| $Cu_{64}Zr_{36}$ (Sim. by Cheng *et al.*[12]) | $10^7$ | 31.67 | 12.83 | | |
| | $10^8$ | 26.00 | | | |
| | $10^9$ | 22.60 | | | |
| $Zr_{50}Cu_{50}$ (Sim. by Wang *et al.*[14]) | $1.5 \times 10^7$ | | 10.5 | | |
| | $1.5 \times 10^8$ | | 8.3 | | |
| | $1.5 \times 10^9$ | | 7.2 | | |
| $Cu_{64}Zr_{36}$ (Sim. by Li *et al.*[69]) | $8.2 \times 10^9$ | | 1.25 | | |
| $Zr_{52.5}Cu_{17.9}Ni_{14.6}Al_{10}Ti_5$ (Exp. by Nieh *et al.*[62]) | 0.0075 | | | 1.05 | 1.07 |
| $Zr_{41.2}Ti_{13.8}Cu_{12.5}Ni_{10}Be_{22.5}$ (Exp. by Lu *et al.*[63]) | 0.75 | | | 2.47 | |

dimension of the shear embryo. Therefore, the critical length scale, as proposed in our model, should be theoretically correlated with a critical elastic energy release. This is analogous to a typical fracture problem, i.e., a critical crack size is often associated with a critical elastic energy release.

## IV. CONCLUSION

To summarize, we show in this paper that the indentation size effect and thus shear band initiation are influenced by the thermal history of a MG. This thermal history dependence as revealed by the spherical indentation can be captured very well by the shear-band initiation model we previously developed. Meanwhile, the variation of the shear-band initiation length scale with the thermal annealing can be rationalized by the well-established model in the earthquake mechanics,[30] thus revealing the mechanistic similarity between shear-band initiation in MGs and earthquake initiation in the earth mantle.[64]

## ACKNOWLEDGMENTS

The research of Y.Y. is supported by the Research Grant Council (RGC), the Hong Kong Government, through the General Research Fund (GRF) with Grant No. CityU11207215.

[1]A. S. Argon, Acta Metall. **27**, 47 (1979).
[2]F. Spaepen, Acta Metall. **25**, 407 (1977).
[3]W. L. Johnson and K. Samwer, Phys. Rev. Lett. **95**, 5501 (2005).
[4]A. J. Cao, Y. Q. Cheng, and E. Ma, Acta Mater. **57**, 5146 (2009).
[5]A. L. Greer, Y. Q. Cheng, and E. Ma, Mater. Sci. Eng., R **74**, 71 (2013).
[6]D. Klaumunzer, A. Lazarev, R. Maass, F. H. D. Torre, A. Vinogradov, and J. F. Loffler, Phys. Rev. Lett. **107**, 185502 (2011).
[7]P. F. Guan, M. W. Chen, and T. Egami, Phys. Rev. Lett. **104**, 205701 (2010).
[8]C. T. Liu, L. Heatherly, D. S. Easton, C. A. Carmichael, J. H. Schneibel, C. H. Chen, J. L. Wright, M. H. Yoo, J. A. Horton, and A. Inoue, Metall. Mater. Trans. A **29**, 1811 (1998).
[9]F. Shimizu, S. Ogata, and J. Li, Acta Mater. **54**, 4293 (2006).
[10]C. A. Volkert, A. Donohue, and F. Spaepen, J. Appl. Phys. **103**, 083539 (2008).
[11]D. C. Jang and J. R. Greer, Nat. Mater. **9**, 215 (2010).
[12]Y. Q. Cheng and E. Ma, Acta Mater. **59**, 1800 (2011).
[13]D. Tonnies, K. Samwer, P. M. Derlet, C. A. Volkert, and R. Maass, Appl. Phys. Lett. **106**, 171907 (2015).
[14]S. Wang, Y. F. Ye, B. A. Sun, C. T. Liu, S. Q. Shi, and Y. Yang, J. Mech. Phys. Solids **77**, 70 (2015).
[15]C. E. Packard and C. A. Schuh, Acta Mater. **55**, 5348 (2007).
[16]J. Ding, Y. Q. Cheng, and E. Ma, Appl. Phys. Lett. **104**, 1912 (2014).
[17]Z. Wang, B. A. Sun, H. Y. Bai, and W. H. Wang, Nat. Commun. **5**, 5823 (2014).
[18]Z. Lu, W. Jiao, W. H. Wang, and H. Y. Bai, Phys. Rev. Lett. **113**, 5501 (2014).
[19]L. S. Huo, J. F. Zeng, W. H. Wang, C. T. Liu, and Y. Yang, Acta Mater. **61**, 4329 (2013).
[20]J. C. Ye, J. Lu, C. T. Liu, Q. Wang, and Y. Yang, Nat. Mater. **9**, 619 (2010).
[21]Z. Y. Liu, Y. Yang, and C. T. Liu, Acta Mater. **61**, 5928 (2013).
[22]Y. Yang, J. F. Zeng, A. Volland, J. J. Blandin, S. Gravier, and C. T. Liu, Acta Mater. **60**, 5260 (2012).
[23]J. Ding, S. Patinet, M. L. Falk, Y. Q. Cheng, and E. Ma, Proc. Natl. Acad. Sci. U. S. A. **111**, 14052 (2014).
[24]Y. H. Liu, D. Wang, K. Nakajima, W. Zhang, A. Hirata, T. Nishi, A. Inoue, and M. W. Chen, Phys. Rev. Lett. **106**, 5504 (2011).
[25]Y. F. Ye, S. Wang, J. Fan, C. T. Liu, and Y. Yang, Intermetallics **68**, 5 (2016).
[26]Y. C. Hu, P. F. Guan, M. Z. Li, C. T. Liu, Y. Yang, H. Y. Bai, and W. H. Wang, Phys. Rev. B **93**, 214202 (2016).
[27]Z. Y. Liu, M. W. Chen, C. T. Liu, and Y. Yang, Appl. Phys. Lett. **104**, 1901 (2014).
[28]H. J. Leamy, H. S. Chen, and T. T. Wang, Metall. Trans. **3**, 699 (1972).
[29]H. Chen, Y. He, G. J. Shiflet, and S. J. Poon, Nature **367**, 541 (1994).
[30]K. Uenishi and J. R. Rice, J. Geophys. Res.: Solid Earth **108**, 17 (2003).
[31]J. J. Lewandowski, W. H. Wang, and A. L. Greer, Philos. Mag. Lett. **85**, 77 (2005).
[32]G. Kumar, D. Rector, R. D. Conner, and J. Schroers, Acta Mater. **57**, 3572 (2009).
[33]W. H. Wang, C. Dong, and C. H. Shek, Mater. Sci. Eng., R **44**, 45 (2004).
[34]Z. Y. Liu, Y. Yang, S. Guo, X. J. Liu, J. Lu, Y. H. Liu, and C. T. Liu, J. Alloys Compd. **509**, 3269 (2011).
[35]H. Bei, Z. P. Lu, and E. P. George, Phys. Rev. Lett. **93**, 125504 (2004).
[36]C. E. Packard, E. R. Homer, N. Al-Aqeeli, and C. A. Schuh, Philos. Mag. **90**, 1373 (2010).
[37]J. P. Chu, J. S. C. Jang, J. C. Huang, H. S. Chou, Y. Yang, J. C. Ye, Y. C. Wang, J. W. Lee, F. X. Liu, P. K. Liaw, Y. C. Chen, C. M. Lee, C. L. Li, and C. Rullyani, Thin Solid Films **520**, 5097 (2012).
[38]L. Tian, Y. Q. Cheng, Z. W. Shan, J. Li, C. C. Wang, X. D. Han, J. Sun, and E. Ma, Nat. Commun. **3**, 609 (2012).
[39]J. C. Ye, J. P. Chu, Y. C. Chen, Q. Wang, and Y. Yang, J. Appl. Phys. **112**, 3516 (2012).
[40]C. Q. Chen, Y. T. Pei, and J. T. M. De Hosson, Acta Mater. **58**, 189 (2010).
[41]A. Bharathula, S.-W. Lee, W. J. Wright, and K. M. Flores, Acta Mater. **58**, 5789 (2010).
[42]A. R. Yavari, K. Georgarakis, W. J. Botta, A. Inoue, and G. Vaughan, Phys. Rev. B **82**, 172202 (2010).
[43]J. C. Ye, J. Lu, Y. Yang, and P. K. Liaw, J. Mater. Res. **24**, 3465 (2009).
[44]H. Guo, P. F. Yan, Y. B. Wang, J. Tan, Z. F. Zhang, M. L. Sui, and E. Ma, Nat. Mater. **6**, 735 (2007).
[45]Y. W. Mai and B. R. Lawn, Ann. Rev. Mater. Sci. **16**, 415 (1986).
[46]J. H. Perepezko, S. D. Imhoff, M. W. Chen, J. Q. Wang, and S. Gonzalez, Proc. Natl. Acad. Sci. U. S. A. **111**, 3938 (2014).
[47]Y. F. Shi, Appl. Phys. Lett. **96**, 1909 (2010).
[48]B. E. Schuster, Q. Wei, T. C. Hufnagel, and K. T. Ramesh, Acta Mater. **56**, 5091 (2008).
[49]B. E. Schuster, Q. Wei, M. H. Ervin, S. O. Hruszkewycz, M. K. Miller, T. C. Hufnagel, and K. T. Ramesh, Scr. Mater. **57**, 517 (2007).
[50]X. L. Wu, Y. Z. Guo, Q. Wei, and W. H. Wang, Acta Mater. **57**, 3562 (2009).
[51]D. Jang, C. T. Gross, and J. R. Greer, Int. J. Plast. **27**, 858 (2011).
[52]W. J. Wright, M. W. Samale, T. C. Hufnagel, M. M. LeBlanc, and J. N. Florando, Acta Mater. **57**, 4639 (2009).
[53]S. X. Song, X. L. Wang, and T. G. Nieh, Scr. Mater. **62**, 847 (2010).
[54]S. X. Song and T. G. Nieh, Intermetallics **17**, 762 (2009).
[55]C. A. Schuh, A. C. Lund, and T. G. Nieh, Acta Mater. **52**, 5879 (2004).
[56]D. Tönnies, R. Maaß, and C. A. Volkert, Adv. Mater. **26**, 5715 (2014).
[57]M. Q. Jiang, W. H. Wang, and L. H. Dai, Scr. Mater. **60**, 1004 (2009).
[58]Y. Zhang and A. L. Greer, Appl. Phys. Lett. **89**, 1907 (2006).
[59]G. P. Zhang, Y. Liu, and B. Zhang, Scr. Mater. **54**, 897 (2006).
[60]Y. Q. Cheng, A. J. Cao, and E. Ma, Acta Mater. **57**, 3253 (2009).
[61]Y. Q. Cheng, A. J. Cao, H. W. Sheng, and E. Ma, Acta Mater. **56**, 5263 (2008).
[62]T. G. Nieh, J. Wadsworth, C. T. Liu, T. Ohkubo, and Y. Hirotsu, Acta Mater. **49**, 2887 (2001).
[63]J. Lu, G. Ravichandran, and W. L. Johnson, Acta Mater. **51**, 3429 (2003).
[64]Q. Wang, S. T. Zhang, Y. Yang, Y. D. Dong, C. T. Liu, and J. Lu, Nat. Commun. **6**, 7876 (2015).
[65]Y. H. Liu, C. T. Liu, W. H. Wang, A. Inoue, T. Sakurai, and M. W. Chen, Phys. Rev. Lett. **103**, 5504 (2009).
[66]Y. Shi and M. L. Falk, Acta Mater. **55**, 4317 (2007).
[67]C. C. Wang, J. Ding, Y. Q. Cheng, J. C. Wan, L. Tian, J. Sun, Z. W. Shan, J. Li, and E. Ma, Acta Mater. **60**, 5370 (2012).
[68]J. R. Greer and J. T. M. De Hosson, Prog. Mater. Sci. **56**, 654 (2011).
[69]Q. K. Li and M. Li, Appl. Phys. Lett. **88**, 1903 (2006).